ISME

Iranian Journal of Mechanical Engineering
The Iranian Society of Mechanical Engineers
Research Paper

DOI: 10.30506/JMEE.2022.527580.1256

Finite Difference Analysis of Transient Flow Analysis of Casson Magneto-nanofluid over a Vertical Porous Conical Plate under the Influence of Thermal Radiation

M. G. Sobamowo[*]
Assistant Professor

In this work, finite difference method is applied to two-dimensional transient heat and mass transfer of Casson nanofluid past an isothermal vertical conical plate embedded in a porous media under the influences of thermal radiation and magnetic field. The results of the numerical computations and simulations show that the temperature and concentration of the fluid increase as the Casson fluid and radiation parameters as well as Prandtl and Schmidt numbers increase. As the Grashof number, radiation, buoyancy ratio and flow medium porosity parameters increase, the velocity of the Casson fluid increases. However, it was recorded that the Casson fluid parameter, buoyancy ratio parameter, the Hartmann, Schmidt and Prandtl numbers decrease as the velocity of the flow increases. Also, the time to reach the steady state concentration, the transient velocity, Nusselt number and the local skin-friction decrease as the buoyancy ratio parameter and Schmidt number increase. Further investigations depict that the steady-state temperature and velocity decrease as the buoyancy ratio parameter and Schmidt number increase. Additionally, the results depict the local skin friction, Nusselt and Sherwood numbers decrease as the Schmidt number increases. Though, the local Nusselt number increases as the buoyancy ratio parameter increases. It was established that near the leading edge of the plate, the local Nusselt number is not affected by both buoyancy ratio parameter and Schmidt number.

Keywords: Finite difference method, Transient Free convection, Casson Nanofluid, Thermal radiation, Mass transfer.

1 Introduction

Free convection flows are widely applied in aeronautics, reactor fluidization, glass-fiber production processes, aerodynamic, cooling of gas turbine rotor blades, drawing of a polymer sheet, foodstuff processing, melt spinning, mechanical forming processes, cooling of metallic plates, wire and fiber coating, extrusion of plastic sheets, continuous casting, rolling, annealing, and tinning of copper wires. In these various applications, the analysis of fluid flow and heat transfer is very essential because the quality of products in the processes depends considerably on the flow and heat transfer characteristics [1-11]. Different analytical and numerical methods have also been applied to the analyses of the flow and heat transfer models. Parameter

[*] Corresponding Author, Department of Mechanical Engineering, University of Lagos, Akoka, Lagos State, Nigeria, mikegbeminiyi@gmail.com

Receive: 2021/04/03 Accepted: 2022/03/23

differentiation method was used by Na and Habib [12] while Merkin [13] presented the similarity solutions for free convection on a vertical plate. Merkin and Pop [14] and Ali et al. [15] applied numerical methods for the flow process. Homotopy analysis method and spectral local linearization approach were adopted by Motsa et al. [16,17] to analyze the free convection boundary layer flow with heat and mass transfer. Also, with the aids of homotopy analysis method, Ghotbi et al. [18] presented the analytical solutions to the free convection flow. In recent times, studies of flow over conical surfaces have been presented [19-36]. However, most of these studies which are based on time invariant that focused on the free convection currents caused by the temperature difference. It should be stated that the flow is also affected by the differences in concentration on material constitution such as seen in atmospheric flows, chemical processing, formation and dispersion of fog, distributive temperature and moisture over agricultural fields. Also, the transient behaviours of the fluids flow before a steady state is reached should be well investigated. Hence, the study of the transient heat and mass transfer of the fluid over the vertical plate is very much important. Moreover, to the best of the authors knowledge, a study on implicit finite difference analysis of transient behaviours of free convection boundary-layer flow, heat and mass transfer of Casson nanofluids over a vertical plate under the influences of thermal radiation, magnetic field, flow medium porosity and nanoparticles has not been presented in literature. Therefore, the transient magnetohydrodynamics free convection heat and mass transfer of Casson nanofluid past an isothermal vertical conical plate embedded in a porous media subjected to thermal radiation is studied using implicit finite difference scheme of Crank-Nicolson type. The numerical solutions are used to carry out parametric studies. The graphical results are presented and discussed.

2 Problem Formulation and Mathematical analysis

Consider a two-dimensional unsteady free-convection flow, heat and mass transfer of a Casson nanofluid over a vertical conical plate embedded in a porous media and parallel to the direction of the generating body force as shown in Fig. (1).

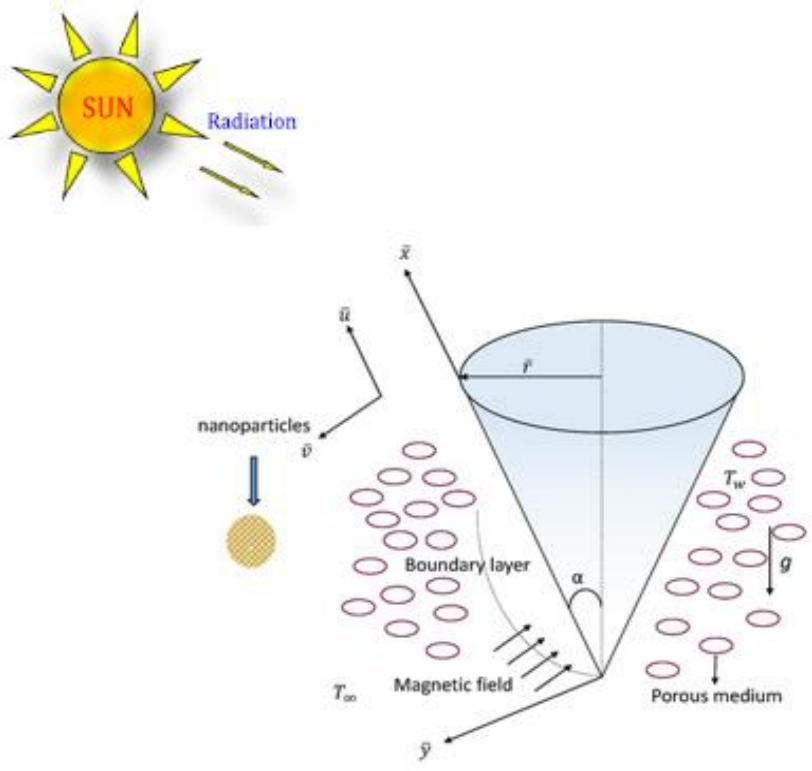

Figure 1 Free convection flow of a Casson fluid over a vertical cone

In order to set up the flow, heat and mass transfer of the Casson nanofluid, the following assumptions are made:

i. The flow is incompressible and laminar
ii. The heat transfer from the plate to the fluid is proportional to the local surface temperature
iii. Pressure is uniform across the boundary layer and Boussinesq approximation is used
iv. The thermal diffusion and diffusion thermal effects which are called the Soret and Dufour effects, respectively are insignificant and they are therefore negligible.
v. The effect of viscous dissipation on the fluid flow process is negligible
vi. There is no chemical reaction taking place in the mass of the fluid.

Taken x-coordinate to be directed upward along the plate in the flow direction and y-coordinate is taken normal to the plate. Then under the stated assumptions, the governing equation of the flow, heat and mass transfer could be written as [44-45]

$$\frac{\partial\left(\bar{r}\,\bar{u}\right)}{\partial\bar{x}}+\frac{\partial\left(\bar{r}\,\bar{v}\right)}{\partial\bar{y}}=0 \tag{1}$$

$$\begin{aligned}&\rho_{nf}\left(\frac{\partial\bar{u}}{\partial\bar{t}}+\bar{u}\frac{\partial\bar{u}}{\partial\bar{x}}+\bar{v}\frac{\partial\bar{u}}{\partial\bar{y}}\right)=\left(1+\frac{1}{\gamma}\right)\mu_{nf}\frac{\partial^2\bar{u}}{\partial\bar{y}^2}\\&+g\left(\rho\beta\right)_{nf}\left(\bar{T}-\bar{T}_\infty\right)cos\gamma+g\left(\rho\beta^*\right)_{nf}\left(\bar{C}-\bar{C}_\infty\right)cos\gamma-\sigma_m B_o^2\bar{u}-\frac{\mu\bar{u}}{K_p}\end{aligned} \tag{2}$$

$$\left(\rho c_p\right)_{nf}\left(\frac{\partial\bar{T}}{\partial\bar{t}}+\bar{u}\frac{\partial\bar{T}}{\partial\bar{x}}+\bar{v}\frac{\partial\bar{T}}{\partial\bar{y}}\right)=k_{nf}\frac{\partial^2\bar{T}}{\partial\bar{y}^2}-\frac{\partial q_r}{\partial\bar{y}} \tag{3}$$

$$\left(\frac{\partial\bar{C}}{\partial\bar{t}}+\bar{u}\frac{\partial\bar{C}}{\partial\bar{x}}+\bar{v}\frac{\partial\bar{C}}{\partial\bar{y}}\right)=D_{nf}\frac{\partial^2\bar{C}}{\partial\bar{y}^2} \tag{4}$$

r is the radius of the vertical cone.

In this work, we adopt a conditions that the plate and the fluid are initially at the same concentration and temperature level that is the same in the fluid everywhere. Then at time $t > 0$, the plate temperature is suddenly raised to T_w, and the concentration level near the plate is also raised to C_w, which are thereafter maintained constant. Therefore, the initial condition is given as

$$\bar{t}\le 0,\quad \bar{u}=0,\quad \bar{v}=0,\quad \bar{T}=T_\infty\quad \bar{C}=C_\infty,\ at\quad 0\le\bar{x}\le L,\ \bar{y}\ge 0 \tag{5}$$

And the appropriate boundary conditions under no slip conditions are given as

$$\bar{t}>0,\quad \bar{u}=0,\quad \bar{v}=0,\quad \bar{T}=T_\infty\quad \bar{C}=C_\infty,\ at\quad \bar{x}=0,\ \bar{y}\ge 0 \tag{6a}$$

$$\bar{t}>0,\quad \bar{u}=0,\quad \bar{v}=0,\quad \bar{T}=T_\infty\quad \bar{C}=C_\infty,\ at\quad \bar{x}=L,\ \bar{y}\ge 0 \tag{6b}$$

$$\bar{t}>0,\quad \bar{u}=0,\quad \bar{v}=0,\quad \bar{T}=T_w\quad \bar{C}=C_w,\ at\quad \bar{x}\ge 0,\ \bar{y}=0 \tag{6c}$$

$$\bar{t}>0,\quad \bar{u}=0,\quad \bar{v}=V_\infty,\quad \bar{T}\to T_\infty\quad \bar{C}\to C_\infty,\ at\quad \bar{x}\ge 0,\ \bar{y}\to\infty \tag{6d}$$

The thermal radiation term in Eq. (3) could be linearized using Rosseland's approximation as follows

$$\frac{\partial q_r}{\partial \overline{y}} = -\frac{4\sigma}{3K}\frac{\partial \overline{T}^4}{\partial \overline{y}} \cong -\frac{16\sigma T_s^3}{3K}\frac{\partial^2 \overline{T}}{\partial \overline{y}^2} \tag{7}$$

Substituting Eq. (7) into Eq. (3), we the governing equations of the flow, heat and mass transfer as

$$\left(\rho c_p\right)_{nf}\left(\frac{\partial \overline{T}}{\partial \overline{t}} + \overline{u}\frac{\partial \overline{T}}{\partial \overline{x}} + \overline{v}\frac{\partial \overline{T}}{\partial \overline{y}}\right) = \left(k_{nf} + \frac{16\sigma T_s^3}{3K}\right)\frac{\partial^2 \overline{T}}{\partial \overline{y}^2} \tag{8}$$

Where the various physical and thermal properties in Eqs. (2) and (3) are given as

$$\rho_{nf} = \rho_f\left(1-\phi\right) + \rho_s\phi \tag{9}$$

$$\left(\rho\beta\right)_{nf} = \left(\rho\beta\right)_f\left(1-\phi\right) + \left(\rho\beta\right)_s\phi \tag{10}$$

$$\left(\rho c_p\right)_{nf} = \left(\rho c_p\right)_f\left(1-\phi\right) + \left(\rho c_p\right)_s\phi \tag{11}$$

$$\mu_{nf} = \frac{\mu_f}{\left(1-\phi\right)^{2.5}} \tag{12}$$

$$k_{nf} = k_f\left[\frac{k_s + \left(m-1\right)k_f - \left(m-1\right)\phi\left(k_f - k_s\right)}{k_s + \left(m-1\right)k_f + \phi\left(k_f - k_s\right)}\right] \tag{13}$$

Where *m* in the above Hamilton Crosser's model in Eq. (13) is the shape factor which numerical values for different shapes are given in Table (1).

$$x = \frac{\overline{x}}{L},\ y = \frac{\overline{y}}{L}Gr_L^{1/2}, r = \frac{\overline{r}}{L},\ u = \frac{\rho_{nf}\overline{u}L}{\mu_{nf}Gr_L^{1/2}},\ v = \frac{\rho_{nf}\overline{v}L}{\mu_{nf}Gr_L^{1/4}},\ T = \frac{\overline{T}-T_\infty}{T_w-T_\infty},\ C = \frac{\overline{C}-C_\infty}{C_w-C_\infty},\ \tau = \frac{tv}{L^2}G_{rL}^{1/2},\ Ha = \frac{\sigma B_o^2 L^2}{\mu_{nf}Gr_L^{1/2}}$$
$$Gr_L = \frac{\rho_{nf}^2 g\beta L^3\left(T_w-T_\infty\right)cos\gamma}{\mu_{nf}^2},\ Pr = \frac{\mu_{nf}c_{p,nf}}{k_{nf}},\ R = \frac{k_{nf}K}{4\sigma T_s^3},\ Sc = \frac{\mu_{nf}}{\rho_{nf}D_{nf}},\ \lambda = \frac{\beta^*\left(C_w-C_\infty\right)}{\beta\left(T_w-T_\infty\right)}, \frac{1}{Da} = \frac{L^2}{Gr_L^{1/4}K_p} \tag{14}$$

Table 1 The values of different shapes of nanoparticles [37-42]

S/N	Name	Shape factor (*m*)	Sphericity(ψ)
1	Sphere	3.0	1.000
2	Brick	3.7	0.811
3	Cylinder	4.8	0.625
4	Platelet	5.7	0.526
5	Lamina	16.2	0.185

We now introduce the following non-dimensional quantities
We have the dimensionless forms of the governing equations as

$$\frac{\partial(ru)}{\partial x}+\frac{\partial(rv)}{\partial y}=0 \quad \left(or \quad \frac{\partial u}{\partial x}+\frac{\partial v}{\partial y}+\frac{u}{x}=0\right) \tag{15}$$

$$\frac{\partial u}{\partial t}+u\frac{\partial u}{\partial x}+v\frac{\partial u}{\partial y}=\left(1+\frac{1}{\gamma}\right)\frac{\partial^2 u}{\partial y^2}+T+\lambda C-Hau-\frac{1}{Da}u \tag{16}$$

$$\frac{\partial T}{\partial t}+u\frac{\partial T}{\partial x}+v\frac{\partial T}{\partial y}=\frac{1}{Pr}\left(\frac{3R+4}{3R}\right)\frac{\partial^2 T}{\partial y^2} \tag{17}$$

$$\frac{\partial C}{\partial t}+u\frac{\partial C}{\partial x}+v\frac{\partial C}{\partial y}=\frac{1}{Sc}\frac{\partial^2 C}{\partial y^2} \tag{18}$$

The appropriate initial and boundary conditions are given as

$$\tau\le 0,\quad u=0,\quad v=0,\quad T=T=0\quad C=0\ \ at\ \ 0\le x\le 1,\ y\ge 0 \tag{19}$$

$$\tau>0,\quad u=0,\quad v=0,\quad T=0\quad C=0\ \ at\quad x=0,\ y\ge 0 \tag{20}$$

$$\tau>0,\quad u=0,\quad v=0,\quad T=0\quad C=0,\ at\quad x=1,\ y\ge 0 \tag{21}$$

$$\tau>0,\quad u=0,\quad v=0,\quad T=1\quad C=1,\ at\quad x\ge 0,\ y=0 \tag{22}$$

$$\tau>0,\quad u=0,\quad v=V_\infty,\quad T\to 0\quad C\to 0,\ at\quad x\ge 0,\ y\to\infty \tag{23}$$

3 Finite Difference Analysis of the Fluid Flow, Heat and Mass Transfer Problems

Indisputably, the finite difference method is one of the efficient methods of obtaining numerical solutions to differential equations. The difference scheme could be applied using explicit or implicit schemes. However, the applications of the finite difference scheme to the practical situations depict that the stability and convergence conditions for explicit finite-difference methods become extremely complicated coupled with high computational cost. In order to avoid obviate the inherent problems in the explicit schemes, implicit schemes are recommended. Such schemes permit large time-steps to be used with unconditional stability. Also, the use and the accuracy of finite difference method for the analysis of nonlinear problems has earlier been pointed out by Han et al. [43]. Therefore, in this work, implicit finite difference method of Crank-Nicolson type is used to discretize the systems of coupled non-linear ordinary differential equations combined with the initial and boundary conditions in governing equations (15), (16), (17) and (18) as well as Eq. (19)-(23), respectively. The finite difference forms for the systems of coupled non-linear ordinary differential equations, the initial and boundary conditions are given as

$$\frac{u_{i,j}^{n+1}-u_{i-1,j}^{n+1}+u_{i,j}^{n}-u_{i-1,j}^{n}+u_{i,j-1}^{n+1}-u_{i-1,j-1}^{n+1}+u_{i,j-1}^{n}-u_{i-1,j-1}^{n}}{4\Delta x_i}+\frac{v_{i,j}^{n+1}-v_{i,j-1}^{n+1}+v_{i,j}^{n}-v_{i,j-1}^{n}}{2\overline{\Delta y_j}}$$
$$\frac{u_{i,j}^{n+1}+u_{i,j-1}^{n+1}+u_{i,j}^{n}+u_{i,j-1}^{n}}{4\Delta x_i}=0 \tag{24}$$

$$\left(\frac{u_{i,j}^{n+1}-u_{i,j}^{n}}{\Delta\tau}\right)+\frac{u_{i,j}^{n}}{2}\left(\frac{u_{i,j}^{n+1}-u_{i-1,j}^{n+1}+u_{i,j}^{n}-u_{i-1,j}^{n}}{\Delta x_i}\right)+\frac{v_{i,j}^{n}}{2}\left(\frac{u_{i,j}^{n+1}-u_{i,j-1}^{n+1}+u_{i,j}^{n}-u_{i,j-1}^{n}}{\overline{\Delta y_j}}\right)$$
$$=\left(1+\frac{1}{\gamma}\right)\frac{\left(\Delta y_j^{+}\left(u_{i,j-1}^{n+1}+u_{i,j-1}^{n}\right)-\overline{\Delta y_j}\left(u_{i,j}^{n+1}+u_{i,j}^{n}\right)+\Delta y_j^{-}\left(u_{i,j+1}^{n+1}+u_{i,j-1}^{n}\right)\right)}{\Delta y_j^{+}\overline{\Delta y_j}\Delta y_j^{-}} \tag{25}$$
$$+\left(\frac{T_{i,j}^{n+1}+T_{i,j}^{n}}{2}\right)+N\left(\frac{C_{i,j}^{n+1}+C_{i,j}^{n}}{2}\right)-Ha\left(\frac{u_{i,j}^{n+1}+u_{i,j}^{n}}{2}\right)-\frac{1}{Da}\left(\frac{u_{i,j}^{n+1}+u_{i,j}^{n}}{2}\right)$$

$$\left(\frac{T_{i,j}^{n+1}-T_{i,j}^{n}}{\Delta\tau}\right)+\frac{u_{i,j}^{n}}{2}\left(\frac{T_{i,j}^{n+1}-T_{i-1,j}^{n+1}+T_{i,j}^{n}-T_{i-1,j}^{n}}{\Delta x_i}\right)+\frac{v_{i,j}^{n}}{2}\left(\frac{T_{i,j+1}^{n+1}-T_{i,j-1}^{n+1}+T_{i,j+1}^{n}-T_{i,j+1}^{n}-T_{i,j-1}^{n}}{\overline{\Delta y_j}}\right)$$
$$=\left(\frac{1}{Pr}+R\right)\frac{\left(\Delta y_j^{+}\left(T_{i,j-1}^{n+1}+T_{i,j-1}^{n}\right)-\overline{\Delta y_j}\left(T_{i,j}^{n+1}+T_{i,j}^{n}\right)+\Delta y_j^{-}\left(T_{i,j+1}^{n+1}+T_{i,j-1}^{n}\right)\right)}{\Delta y_j^{+}\overline{\Delta y_j}\Delta y_j^{-}} \tag{26}$$

$$\left(\frac{C_{i,j}^{n+1}-C_{i,j}^{n}}{\Delta\tau}\right)+\frac{u_{i,j}^{n}}{2}\left(\frac{C_{i,j}^{n+1}-C_{i-1,j}^{n+1}+C_{i,j}^{n}-C_{i-1,j}^{n}}{\Delta x_i}\right)+\frac{v_{i,j}^{n}}{2}\left(\frac{C_{i,j+1}^{n+1}-C_{i,j-1}^{n+1}+C_{i,j+1}^{n}-C_{i,j+1}^{n}-C_{i,j-1}^{n}}{\overline{\Delta y_j}}\right)$$
$$=\frac{1}{Sc}\frac{\left(\Delta y_j^{+}\left(C_{i,j-1}^{n+1}+C_{i,j-1}^{n}\right)-\overline{\Delta y_j}\left(C_{i,j}^{n+1}+C_{i,j}^{n}\right)+\Delta y_j^{-}\left(C_{i,j+1}^{n+1}+C_{i,j-1}^{n}\right)\right)}{\Delta y_j^{+}\overline{\Delta y_j}\Delta y_j^{-}} \tag{27}$$

The appropriate initial and boundary conditions in finite difference forms are given as

$$u_{i,j}^{0}=0,\quad v_{i,j}^{0}=0,\quad T_{i,j}^{0}=0\quad C_{i,j}^{0}=0 \tag{28}$$

$$u_{0,j}^{n}=0,\quad v_{0,j}^{n}=0,\quad T_{0,j}^{n}=0\quad C_{0,j}^{n}=0 \tag{29}$$

$$u_{1,j}^{n}=0,\quad v_{1,j}^{n}=0,\quad T_{1,j}^{n}=0\quad C_{1,j}^{n}=0 \tag{30}$$

$$u_{i,0}^{n}=0,\quad v_{i,0}^{n}=0,\quad T_{i,0}^{n}=1\quad C_{i,0}^{n}=1 \tag{31}$$

$$u_{i,L}^{n}=0,\quad v_{i,L}^{n}=V_{\infty},\quad T_{i,L}^{n}=0\quad C_{i,L}^{n}=0 \tag{32}$$

Where

$$\Delta x_j = x_i - x_{i-1}, \quad \Delta y_j = y_i - y_{i-1}, \quad \Delta y_j^+ = y_{i+1} - y_i$$
$$\overline{\Delta y_j} = y_{i+1} - y_{i-1}, \quad \Delta y_j^- = y_i - y_{i-1}$$

The implicit finite difference scheme is used for the Cartesian coordinate. The rectangular region of the integration (Fig. 2) considered varies from 0 to *1* and *y* varying from *0* to *15*. It *is* taken in this study that y_{max} lies well outside the momentums, energy and concentration boundary layers. It should be pointed out that after some preliminary investigations, the maximum of y was chosen as 15. This value is arrived at in order to make the boundary conditions in Equs. (19) and (20) to be satisfied within the tolerance limit of 10^{-5}.

For the rectangular region considered, the *x*- and *y*-directions are divided into M and L grid spacings, respectively as shown in Fig. (2). In order to reduce the computational time, variable mesh sizes are used in the *x*- and *y*-directions as follows

$$\Delta x = \begin{cases} 0.02 & 0 \le x \le 0.10 \\ 0.06 & 0.10 \le x \le 0.40 \\ 0.10 & 0.4 \le x \le 1.00 \end{cases} \tag{33}$$

$$\Delta y = \begin{cases} 0.10 & 0 \le y \le 2.0 \\ 0.50 & 2.0 \le y \le 15 \end{cases} \tag{34}$$

$$\Delta \tau = 0.05 \tag{35}$$

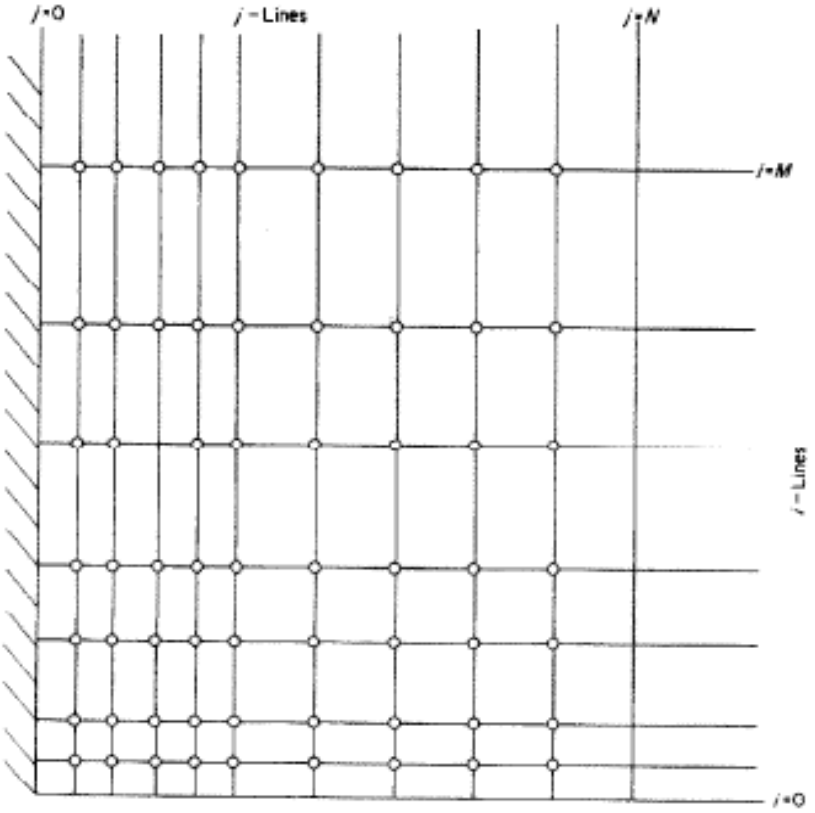

Figure 2 The finite difference space grid for a non-uniform grid system

It should be stated that the subscripts *i* designates the grid points with x-direction while *j* designates the grid points y-direction as shown in Fig. (2). The superscript *n* represents a value of time in t-direction. The velocity, temperature and concentration distributions at all interior nodal points are computed by successive applications of the above finite difference equations in Eqs. (24), (25), (26) and (27) along with the initial and boundary conditions in Eqs. (28) – (32). The process of the computations is explained below.
From the initial conditions in Eqs. (28) – (32), the initial values (at $t = 0$) of u, v, T and C are known at all grid points. For the subsequent computations, it should be stated that during any one-time step, the coefficients $u_{i,j}^{n}$ and $v_{i,j}^{n}$ appearing in the finite difference equations are treated as constants. Using the known values at previous time level (n), the computations of u, v, T, and C at time level ($n + 1$) are calculated as follows:
At every internal nodal point on a particular *i – level*, the finite difference equation in Eq. (27) constitutes a tri-diagonal system of equations which is solved by Thomas algorithm as explained by Carnahan et al. [44]. Therefore, the values of C are determined at every nodal point on a particular *i-level* at *(n+ 1)th time level*. In the same way, the values of T are computed using the finite difference Eq. (26). Substituting the values of C and T at *(n +1)th time* level in the finite difference Eq. (25), the values of u at (n+ 1)th time level are found. Having determined the values of C, T and u on a particular *i – level*, with the aid of the finite difference Eq. (24) at every nodal point on a particular *i – level* at *(n +1)th time level*, the values of v are calculated explicitly. This process is repeated for various *i – levels*. Thus, the values of C, T, u and v are known at all grid points in the rectangular region at *(n+ 1)th* time level. The computations are carried out till the steady state is reached. In this present study, it is assumed that the steady state solution is reached, when the absolute difference between the values of u, T and C at two consecutive time steps are less than 10^{-5} at all grid points.

4 Flow, heat and mass transfer parameters of engineering interests

In addition to the determination of the velocity, temperature and concentration distributions, it is often desirable to compute other physically important quantities (such as shear stress, drag, heat transfer and mass transfer rates) associated with the free convection flow, heat transfer and mass transfer problems. Consequently, flow, heat and mass transfer parameters are computed [30, 44,45].

4.1 Fluid flow parameter

The local skin-friction are derived as

$$\tau_L = \frac{1}{Gr_L^{1/4}} \left(\frac{\partial u}{\partial y} \right)\Bigg|_{y=0} \tag{36}$$

4.2 Heat transfer parameter

The local Nusselt number are given as

$$Nu_{xL} = -\left(\frac{\partial T}{\partial y} \right)\Bigg|_{y=0} xGr_L^{1/2} \tag{37}$$

4.3 Mass transfer parameter

The Sherwood are developed as

$$Sh_{xL} = -\left(\frac{\partial C}{\partial y}\right)\Bigg|_{y=0} xGr_L^{1/4} \tag{38}$$

The derivatives in Eq. involved in the Eqs. (36), (37) and (38) are evaluated using five-point approximation formula while the integrals are evaluated using Newton–Cotes closed integration formula.

5 Results and Discussion

The results of the simulations are presented in this section and the effects of the various model parameters are presented.

5.1 Grid Independence Test and Code Verification

The grid independence or convergence test was carried out using 20, 40, 60, 80, 100, 120, 140, 160 and 180 numbers of points. It was found that after 180 points, there is no appreciable change in the results and the results converged or become independent of the number of grid points. It is observed that in the same domain the accuracy is not affected even if the numbers of points are increased. The grid independency test shows that 180 grid points are adequate to describe the flow processes. Also, the results obtained for lesser number of points are of sufficient accuracy. Therefore, 180 points provided a very good accuracy for the velocity, temperature, and concentration gradient values as they accurately describe the flow and heat transfer processes.

Using the results available in literature, the solution procedure, in the form of an in-house computational fluid dynamics code, have been verified successfully as shown in Table (2). Therefore, this method has been proven to be adequate and give accurate results for boundary layer problems as presented in this work.

For the subsequent simulations in sections (5.2) to (5.9), the variations in the parameters are given as R = 0.2 – 0.4, Pr = 10 – 500, Sc = 0.30 – 0.50, Da = 20 -200, Gr = 1.00 – 4.00, Ha = 0 – 0.6, N = 0.0 – 3.0, γ = 0.2 – 0.8 and τ = 0.20 - 1.80.

5.2 Effects of Casson parameter on the fluid velocity, temperature and concentration distributions

The effects of Casson parameter on the flow velocity, temperature and concentrations profiles

Table 2 8 Comparison of results at x=1, R=0, Ha=0, $\lambda = 0$, Da=100

Heat transfer parameter	Flow and Heat transfer Parameters of interest	Hering [30]	Thandapani et al. [44]	Balla and Naikoti [45]	Present study
Pr =0.1	Skin friction	1.0960	1.10189	1.096308	1.09632
	Nusselt number	0.2113	0.22509	0.226207	0.226208
Pr=0.7	Skin friction	0.8195	0.82566	0.81945	0.81945
	Nusselt number	0.4511	0.44771	0.451898	0.45191

of the nanofluid are shown in Fig. (3a), (3b) and (3c), respectively. The figures depict that the flow velocity of the nanofluid near the plate decreases as the Casson parameter increases as illustrated in Fig. (3a). The trend in the figure could explained that, physically, increasing values of Casson parameter develop the viscous forces which in consequent retards the flow of the and thereby reduced the flow velocity. It could be established from the results that the temperature as well as the concentration of the fluid increase as the Casson fluid parameter increase as shown in Fig. (3b) and (3c).

5.3 Effects of radiation parameter on the fluid velocity, temperature and concentration distributions

Fig. (4a. 4b) and (4c) show that the viscous, thermal and concentration boundary layers increase with the increase of radiation parameter, R. It is shown that increase in radiation parameter causes the velocity of the fluid to increase. This is because as the radiation parameter is increased, the absorption of radiated heat from the heated plate releases more heat energy released to the fluid and the resulting temperature increases the buoyancy forces in the boundary layer which also increases the fluid motion and the momentum boundary layer thickness accelerates. This is expected, because the considered radiation effect within the boundary layer increases the motion of the fluid which increases the surface frictions.

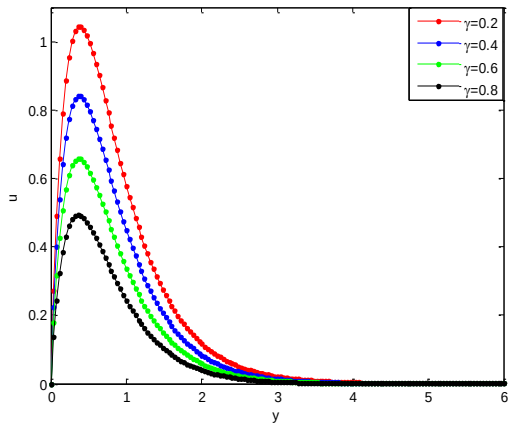

Figure 3a. Effects of Casson parameter on the velocity profile of the Casson nanofluid

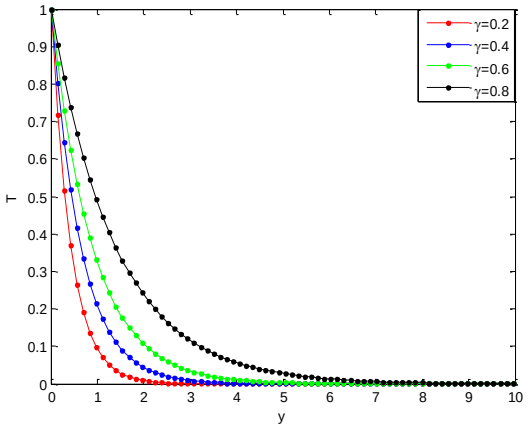

Figure 3b. Effects of Casson parameter on temperature profile of the Casson nanofluid

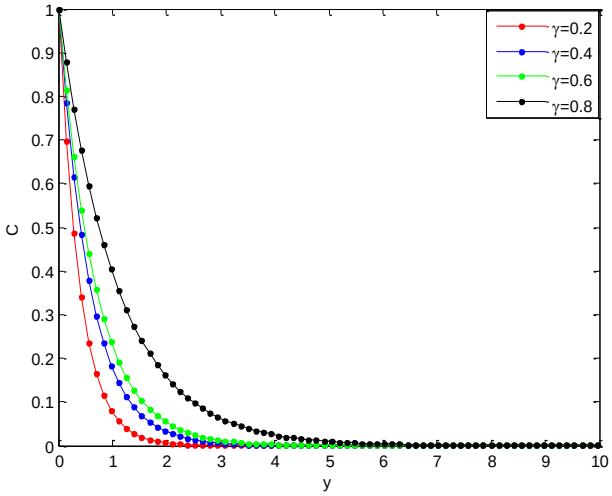

Figure 3c. Effects of Casson parameter on concentration profile Of the Casson nanofluid

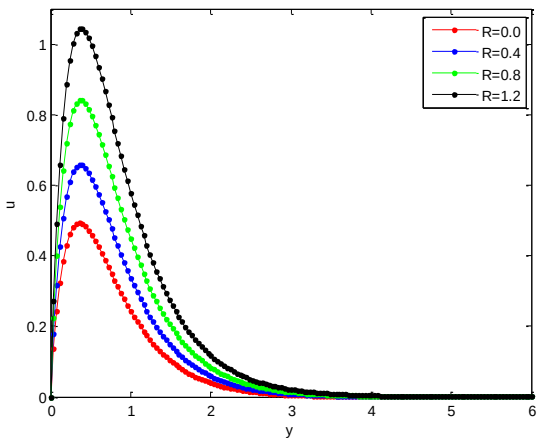

Figure 4a. Effects of radiation parameter on the velocity profile of the Casson nanofluid

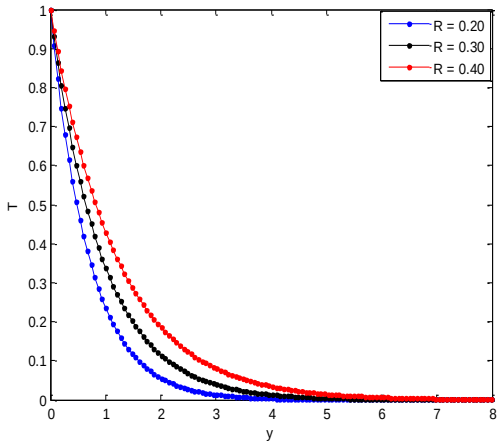

Figure 4b. Effects of radiation parameter on temperature profile of the Casson nanofluid

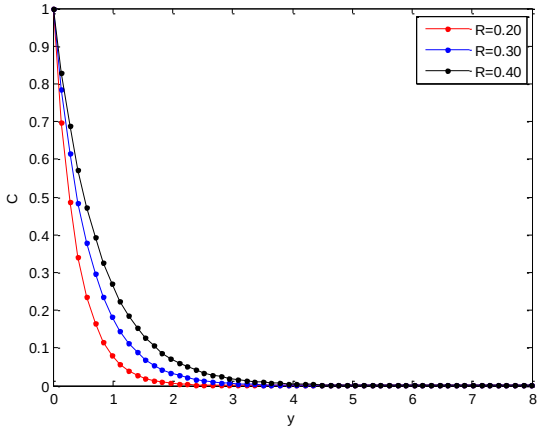

Figure 4c. Effects of radiation parameter on concentration profile of the Casson nanofluid

5.4 Effects of nanoparticle shape on the fluid velocity, temperature and concentration distributions

The use of nanoparticles in the fluids exhibited better properties relating to the heat transfer of fluid than heat transfer enhancement through the use of suspended millimeter- or micrometer-sized particles which potentially cause some severe problems, such as abrasion, clogging, high pressure drop, and sedimentation of particles. The very low concentrations applications and nanometer sizes properties of nanoparticles in basefluid prevent the sedimentation in the flow that may clog the channel. It should be added that the theoretical prediction of enhanced thermal conductivity of the basefluid and prevention of clogging, abrasion, high pressure drop and sedimentation through the addition of nanoparticles in basefluid have been supported with experimental evidences in literature.

Fig. (5a), (5b) and (5c) show the influence of the shape of nanoparticle on the flow velocity, temperature and concentrations profiles of the nanofluid. It is observed that lamina shaped nanoparticle carries maximum velocity whereas spherical shaped nanoparticle has better enhancement on heat transfer than other nanoparticle shapes. In fact, it is in accordance with the physical expectation since it is well known that the lamina nanoparticle has greater shape factor than other nanoparticles of different shapes, therefore, the lamina nanoparticle comparatively gains maximum temperature than others. The velocity decrease is maximum in spherical nanoparticles when compared with other shapes. The enhancement observed at lower volume fractions for non-spherical particles is attributed to the percolation chain

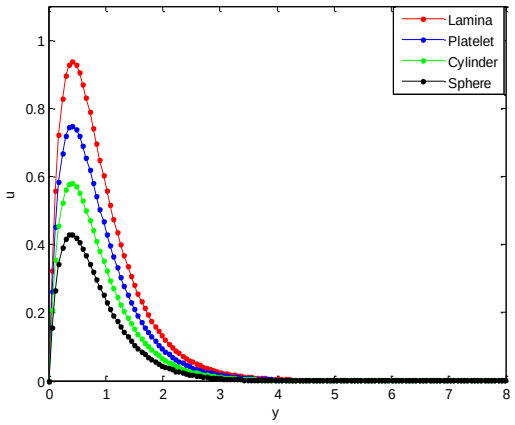

Figure 5a. Effect of nanoparticle shape on velocity distribution of the nanofluid

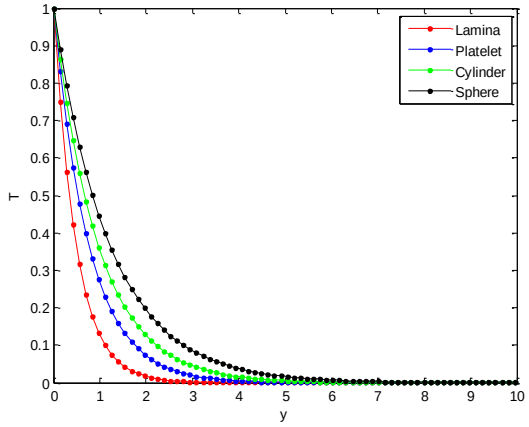

Figure 5b. Effects of nanoparticle shape on temperature distribution of nanofluid

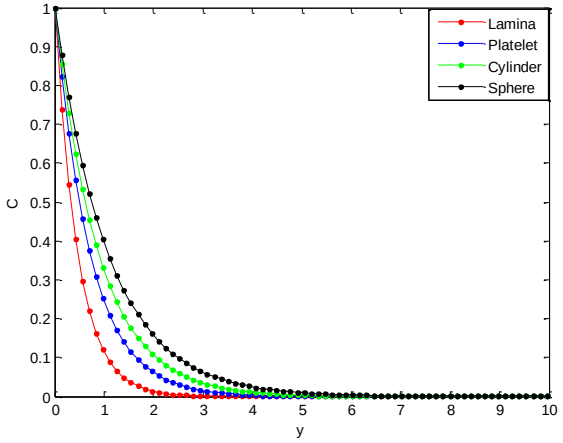

Figure 5c. Effects of nanoparticle shape on concentration distribution

formation, which perturbs the boundary layer and thereby increases the local Nusselt number values. The results show that the maximum decrease in velocity and maximum increase in temperature are caused by lamina, platelets, cylinder and sphere, respectively. It is also observed that irreversibility process can be reduced by using nanoparticles, especially the spherical particles. This can potentially result in higher enhancement in the thermal conductivity of a nanofluid containing elongated particles compared to the one containing spherical nanoparticle, as exhibited by the experimental data in the literature. It is therefore required that that proper choice of nanoparticles should made as this will be helpful in controlling fluid flow, heat and mass transfer processes.

5.5 Effect of Prandtl number on the fluid velocity, temperature and concentration distributions

The figures also show the effects of Prandtl number (Pr) on the velocity and temperature profiles are shown in Fig. (6a), (6b) and 6c, respectively. It is indicated that the velocity of the Casson nanofluid decreases as the Pr increases but the temperature of the nanofluid increases as the Pr increases. This is because the nanofluid with higher Prandtl number has a relatively low thermal conductivity, which reduces conduction, and thereby reduces the thermal boundary-layer thickness, and as a consequence, increases the heat transfer rate at the surface. For the case of the fluid velocity that decreases with the increase of Pr, the reason is that fluid of the higher Prandtl number means more viscous fluid, which increases the boundary-layer thickness and thus, reduces the shear stress and consequently, retards the flow of the nanofluid.

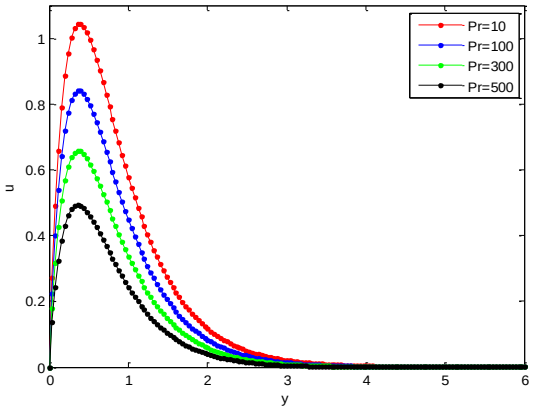

Figure 6a. Effects of Prandtl number on the velocity profile

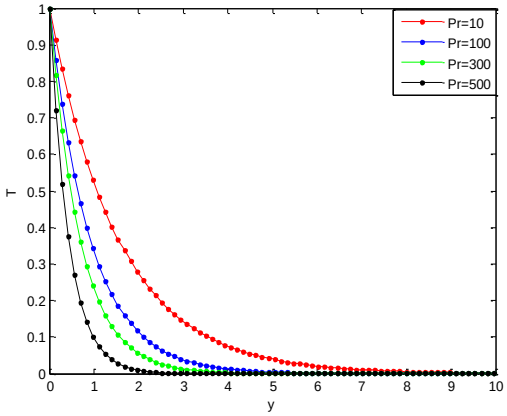

Figure 6b. Effects of Prandtl number on temperature profile

Also, it can be seen that the velocity distribution for small value of Prandtl number consist of two distinct regions. A thin region near the wall of the plate where there are large velocity gradients due to viscous effects and a region where the velocity gradients are small compared with those near the wall. In the later region, the viscous effects are negligible and the flow of fluid in the region can be considered to be inviscid. Also, such region tends to create uniform accelerated flow at the surface of the plate.

5.6 Effect of Schmidt and Grashof numbers on fluid velocity and temperature distributions

Fig. (7a) and (7b) shows the effects of Schmidt number (Sc) on the velocity and concentration profiles of the Casson nanofluid, respectively. Fig. (8) shows that the as Grashof number increases, the velocity of the fluid increases. However, as in the case of the effect of Prandtl number on the velocity and temperature distribution, it is depicted in the figures that the velocity of the nanofluid decreases as the Sc increases but the temperature of the nanofluid increases as the Sc increases. This is because the nanofluid with higher Schmidt number has a relatively low diffusion coefficient, which reduces mass diffusion thereby reduces the concentration boundary-layer thickness, and as a consequence, increases the mass transfer rate at the surface. In Fig. (7a), where the fluid velocity decreases with the increase of Sc, this is because the fluid of the higher Schmidt number means more viscous fluid, which increases the boundary-layer thickness and thus, reduces the shear stress and consequently, retards the flow of the nanofluid. It is also observed that the species concentration decreases with increasing Schmidt number as shown in Fig. (7b). It was also found that the temperature increases with increasing Schmidt number. A further investigation revealed that an increase in the Schmidt number leads to a decrease in Grashof number Gr.

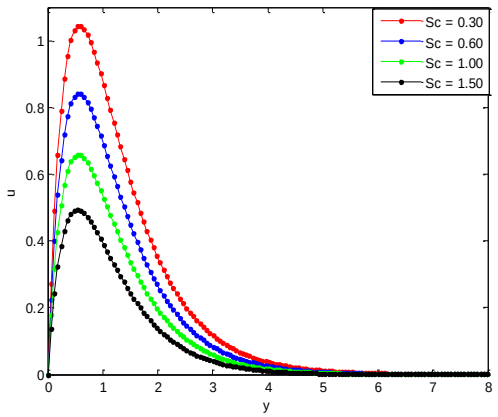

Figure 7a. Effects of Schmidt number on the velocity distribution

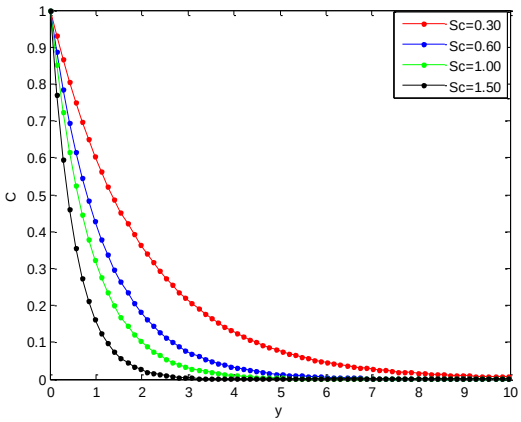

Figure 7b. Effects of Schmidt number on the concentration distribution

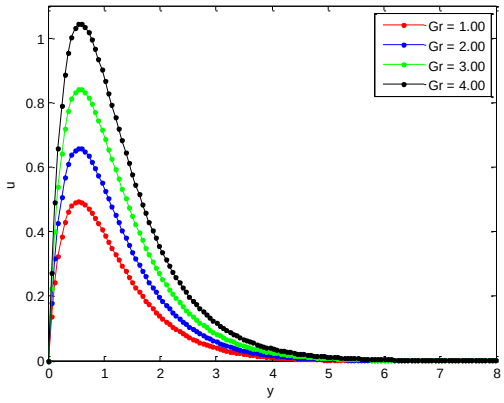

Figure 8. Effects of Grashof number on the velocity distribution

5.7 Effects of Magnetic field and Flow Medium Porosity on Casson nanofluid velocity distributions

Figs. (9) shows the effect of magnetic field on the flow velocity of the fluid. It is revealed that there is a diminution in the velocity field occurs for increasing value of the magnetic field number, Hartmann number (Ha). This confirms the general physical behavior of the magnetic field that say that the fluid velocity depreciates for improved values of Ha. The magnetic field produces Lorentz force which is drag-like force that produces more resistance to the flow and reduces the fluid velocity. So large Ha values implies that the Lorentz force increases and the resistance to the flow increases, and consequently, the velocity of the fluid decreases. Practically, the Lorentz force has a resistive nature which opposes motion of the fluid and as a result heat is produced which increases thermal boundary layer thickness and fluid temperature. The magnetic field tends to make the boundary layer thinner, thereby increasing the wall friction. Consequently, the boundary layer thickness is a decreasing function of Ha. i.e. presence of magnetic field slows fluid motion at boundary layer and hence retards the velocity field.

A porous medium studies is very important in a number of engineering applications such as geophysics, die filling, metal processing, agricultural and industrial water distribution, oil recovery techniques, and injection molding. Therefore, Figs. (10) shows the effect of flow medium porosity on the fluid velocity. As it is illustrated, the fluid velocity increases as the flow medium porosity, Darcy number increases. This is because, as the Darcy number increases, there is less resistance to fluid flow through the flow medium.

Also, it was found that the variations of the flow velocity and the temperature gradient of the fluid are inversely proportional to half of the cone angle, γ increases. It should be noted that as the angle increases, the applied magnetic field decreases. Additional, the skin friction factor in terms of shear stress and heat transfer rate in terms of Nusselt number are decreased.

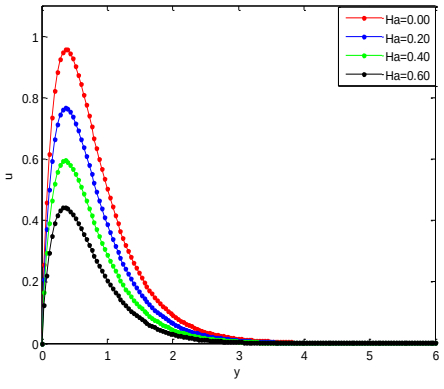

Figure 9. Effects of Hartmann number on the velocity distribution

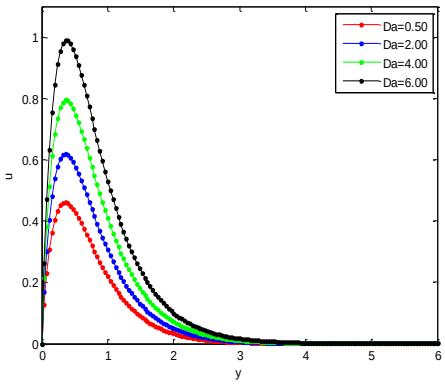

Figure 10 Effects of Darcy number on the concentration distribution

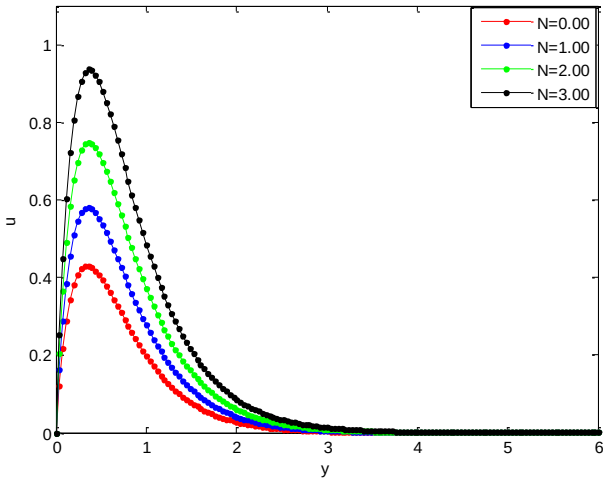

Figure 11a. Effects of buoyancy ratio on the velocity distribution

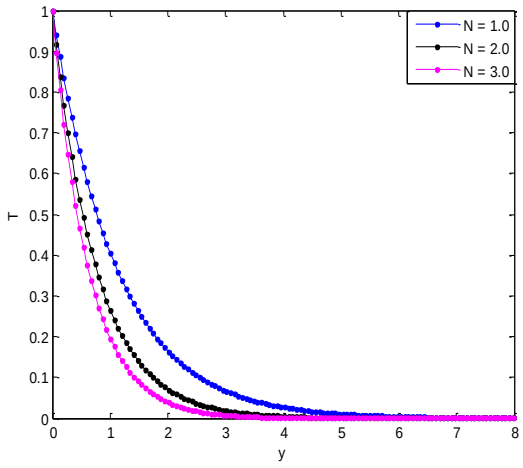

Figure 11b. Effects of buoyancy ratio on the temperature distribution

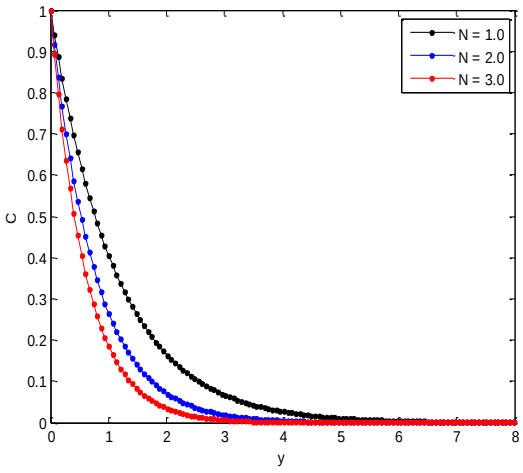

Figure 11c. Effects of buoyancy ratio on the concentration distribution

5.8 Effect of Buoyancy ratio parameter on the fluid velocity, temperature and concentration distributions

Fig (11a), (11b) and (11c) show the impacts of buoyancy ratio parameter (N = λ) on the velocity, temperature and concentration profiles. Fig. (11a) depicts that the as buoyancy ratio parameter increases, the velocity of the fluid increases. However, an increase in buoyancy ratio parameter leads to a decrease in the fluid temperature and concentration as shown in Figs. (11b) and (11c).

5.9 Effect of flow time on the fluid velocity, temperature and concentration distributions

In order to shown the effects of flow time on the velocity, temperature and concentration distributions, Figs. 11a-c are presented Apart from the fact that the velocity, temperature and concentration distributions increase as the flow time increases, the results also shown the effects of the controlling parameters on the time to reach steady state velocity, temperature and concentration. In our further investigations, the required time to reach the steady state concentration, the transient velocity, Nusselt number and the local skin-friction decrease as the buoyancy ratio parameter and Schmidt number increase. Also, the steady-state temperature and velocity decrease as the buoyancy ratio parameter and Schmidt number increase.

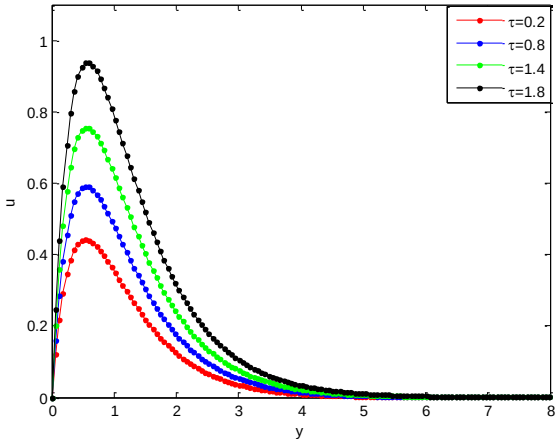

Figure 12a. Effects of flow time on the velocity distribution

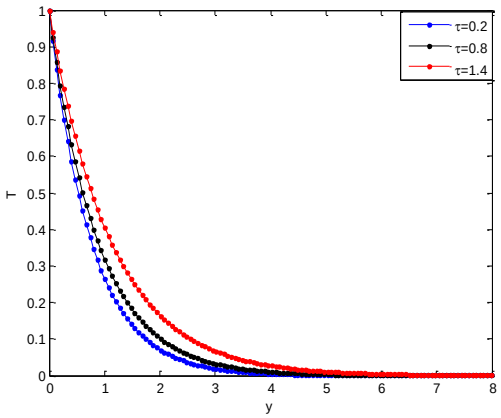

Figure 12b. Effects of flow on the temperature distribution

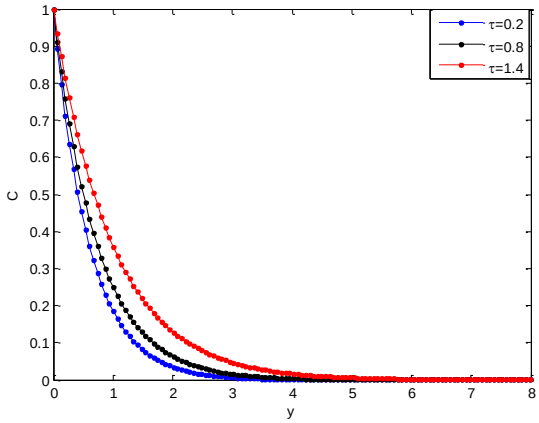

Figure 12c. Effects of flow time on the concentration distribution

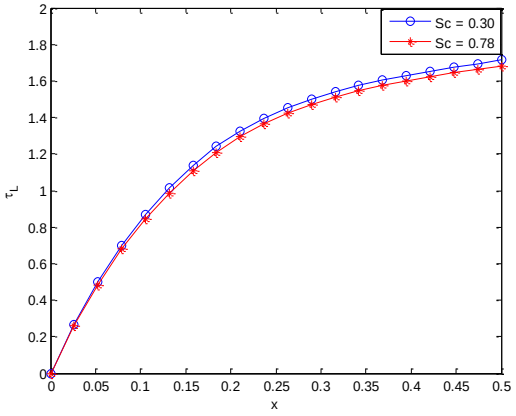

Figure 13 Effects of Schmidt number on local skin friction

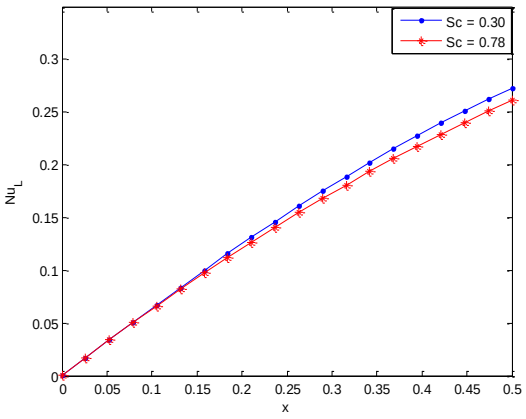

Figure 14 Effects of Schmidt number on Nusselt number

The effects of Schmidt number on local skin friction, Nusselt and Sherwood numbers are shown in Fig. (13), (14) and (15), respectively. The figures reveal that the local skin friction, Nusselt and Sherwood numbers decrease as the Schmidt number increases. An opposite trend was recorded when the impact of the buoyancy ratio parameter on Nusselt number was investigated. In the investigation, it was found that as the local Nusselt number increases as the buoyancy ratio parameter increases. It was shown that at small values of x (near the leading edge of the plate), the local Nusselt number is not affected by both buoyancy ratio parameter and Schmidt number due to the pure diffusion and conduction at the location.

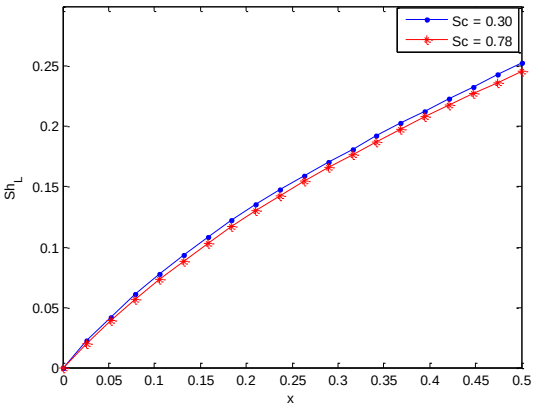

Figure 15 Effects of Schmidt number on Sherwood number

6 Conclusion

In this present study, the transient free convection heat and mass transfer of Casson nanofluid past an isothermal vertical conical plate embedded in a porous media under the influences of thermal radiation and magnetic field have been investigated. The governing systems of nonlinear partial differential equations of the flow, heat and mass transfer processes are solved using implicit finite difference scheme of Crank-Nicolson type. The numerical solutions are used to carry out parametric studies and the follow results were established:

i. The temperature and the concentration of the fluid increase as the Casson fluid and radiation parameters as well as Prandtl and Schmidt numbers increase.

ii. The increase in the Grashof number, radiation, buoyancy ratio and flow medium porosity parameters causes the velocity of the fluid to increase. However, the Casson fluid parameter, buoyancy ratio parameter, the Hartmann (magnetic field parameter), Schmidt and Prandtl numbers decrease as the velocity of the flow increases.

iii. The time to reach the steady state concentration, the transient velocity, Nusselt number and the local skin-friction decrease as the buoyancy ratio parameter and Schmidt number increase.

iv. The steady-state temperature and velocity decrease as the buoyancy ratio parameter and Schmidt number increase.

v. The local skin friction, Nusselt and Sherwood numbers decrease as the Schmidt number increases. However, the local Nusselt number increases as the buoyancy ratio parameter increases.

vi. Following the results in this work, it is believed that the present study will greatly assist in various areas of industrial and engineering applications of the flow problems.

References

[1] Schmidt, E., and Beckmann, W., "Das Temperatur-und Geschwindigkeitsfeld vor Einer wärme Abgebenden Senkrecher Platte bei Batürelicher Convention", Tech. Mech, U. Themodynamik, Bd., 1(10), (1930), 341-349; cont. Bd., 1(11), (1930), 391- 406.

[2] Ostrach, S., "An Analysis of Laminar Free-convection Flow and Heat Transfer about a Fat Plate Parallel to the Direction of the Generating Body Force", NACA Report, 1111, (1953).

[3] Sparrow, E.M., and Gregg, J.L., "Laminar Free Convection from a Vertical Plate with Uniform Surface Heat Flux", Transactions of the American Society of Mechanical Engineers, (Trans. A.S.M.E.), Vol. 78, pp. 435-440, (1956).

[4] Lefevre, E.J., "Laminar Free Convection from a Vertical Plane Surface", 9th International Congress on Applied Mechanics, Brussels, paper I, Vol. 4, pp. 168, (1956).

[5] Sparrow, E.M., and Gregg, J.L., "Similar Solutions for Free Convection from a Nonisothermal Vertical Plate", Transactions of the American Society of Mechanical Engineers, (Trans. A.S.M.E.), Vol. 80, pp. 379-386, (1958).

[6] Stewartson, K., and Jones, L.T., "The Heated Vertical Plate at High Prandtl Number", Journal Aeronautical Sciences, Vol. 24, pp. 379-380, (1957).

[7] Kuiken, H.K., "An Asymptotic Solution for Large Prandtl Number Free Convection, Journal of Engineering Mathematics, Vol. 2, pp. 355-371, (1968).

[8] Kuiken, H.K., "Free Convection at Low Prandtl Numbers", Journal of Fluid Mechanics, Vol. 37(4), pp. 785-798, (1969).

[9] Eshghy, S., "Free-convection Layers at Large Prandtl Number", Journal of Applied Mathematics and Physics, (ZAMP), Vol. 22, pp. 275 -292, (1971).

[10] Roy, S., "High Prandtl Number Free Convection for Uniform Surface Heat Flux", Trans A.S.M.E., Journal of Heat Transfer, Vol. 95(1), pp. 124-126, (1973).

[11] Kuiken, H.K., and Rotem, Z., "Asymptotic Solution for the Plume at Very Large and Small Prandtl Numbers", Journal of Fluid Mechanics, Vol. 45, pp. 585-600, (1971).

[12] Na, T.Y., and Habib, I.S., "Solution of the Natural Convection Problem by Parameter Differentiation", International Journal of Heat and Mass Transfer, Vol. 17, pp. 457–459, (1974).

[13] Merkin, J.H., "A Note on the Similarity Solutions for Free Convection on a Vertical Plate", Journal of Engineering Mathematics, Vol. 19, pp. 189-201, (1985).

[14] Merkin, J.H., and Pop, I., "Conjugate Free Convection on a Vertical Surface", International Journal of Heat and Mass Transfer, Vol. 39, pp. 1527–1534, (1996).

[15] Ali, F.M., Nazar, R., and Arifin, N.M., "Numerical Investigation of Free Convective Boundary Layer in a Viscous Fluid", The American Journal of Scientific Research, No. 5, pp. 13–19, (2009).

[16] Motsa, S.S., Shateyi, S., and Makukula, Z., "Homotopy Analysis of Free Convection Boundary Layer Flow with Heat and Mass Transfer", Chemical Engineering Communications, Vol. 198, No. 6, pp. 783–795, (2011).

[17] Motsa, S.S., Makukula, Z.G., and Shateyi, S., "Spectral Local Linearisation Approach for Natural Convection Boundary Layer Flow", Hindawi Publishing Corporation Mathematical

Problems in Engineering, Article ID 765013, https://doi.org/10.1155/2013/765013, Vol. 2013, pp. 7, (2013).

[18] Ghotbi, A.R., Bararnia, H., Domairry, G., and Barari, A., "Investigation of a Powerful Analytical Method into Natural Convection Boundary Layer Flow", Communications in Nonlinear Science and Numerical Simulation, Vol. 14, No. 5, pp. 2222–2228, (2009).

[19] Alam, M.M., Alim, M.A., and Chowdhury, M.K., "Free Convection from a Vertical Permeable Circular Cone with Pressure Work and Non-uniform Surface Temperature", Nonlinear Analysis Modeling and Control, Vol. 261, pp. 21-32, (2007).

[20] Alamgir, M., "Over-all Heat Transfer from Vertical Cones in Laminar Free Convection: An Approximate Method", Transactions of ASME, Journal of Heat Transfer, Vol. 101, pp. 174-176, (1979).

[21] Alim, M.A., Alam, M.M., and Chowdhury, M.K., "Pressure Work Effect on Natural Convection from a Vertical Circular Cone with Suction and Non-uniform Surface Temperature", Journal of Mechanical Engineering, Vol. 36, pp. 6-11, (2014).

[22] Elbashbeshy, E.M.A., Emam, T.G., and Sayed, E.A., "Effect of Pressure Work on Free Convection Flow from a Vertical Circular Cone with Variable Surface Heat Flux, STROJNICKY CASOPIS, Vol. 63(3), pp. 169-177, (2012).

[23] Hering, R.G., and Grosh, R.J., "Laminar Free Convection from a Non-isothermal Cone", International Journal of Heat and Mass Transfer, Vol. 5(11), pp. 1059-1068, (1962).

[24] Hossain, M.A., and Paul, S.C., "Vertical Permeable Circular Cone with Non-uniform Surface Heat Flux", Heat Mass Transfer, Vol. 37, pp. 167-173, (2001).

[25] Na, T.Y., and Chiou, J.P., "Laminar Natural Convection over a Frustum of a Cone", Applied Scientific Research, Vol. 35, pp. 409-421, (1979).

[26] Roy, S., "Free Convection over a Slender Vertical Cone at High Prandtl Numbers", ASME International Journal of Heat and Mass Transfer, Vol. 101, pp. 174–176, (1974).

[27] Elbashbeshy, E.M.A., Emam, T.G., and Sayed, E.A., "Effect of Pressure Work on Free Convection Flow about a Truncated Cone", International Journal of Physical Sciences, Vol. 1(1), pp. 001-010, (2013).

[28] Thameem Basha, H., Animasaun, I.L., Makinde, O.D., and Sivaraj, R., "Effect of Electromagnetohydrodynamic on Chemically Reacting Nanofluid Flow over a Cone and Plate", Applied Mathematics and Scientific Computing, Trends in Mathematics, Birkhäuser, Cham, pp. 99-107, (2019).

[29] Hering, R.G., and Grosh, R.J., "Laminar Free Convection from a Non-isothermal Cone, International Journal of Heat and Mass Transfer, Vol. 5, pp. 1059–1068, (1962).

[30] Hering, R.G., "Laminar Free Convection from a Non-isothermal Cone at Low Prandtl Number, International Journal of Heat and Mass Transfer, Vol. 8, pp. 1333–1337, (1965).

[31] Pullepu, B., Ekambavananl, K., and Chamkha, A.J., "Unsteady Laminar Natural Convection from a Non-isothermal Vertical Cone", Nonlinear Analysis: Modelling and Control, Vol. 12, No. 4, pp. 525–540, (2007).

[32] Hanafi, H., Shafie, S., and Ullah, S.I., "Unsteady Free Convection Flow of Nanofluid with Dissipation Effect over a Non-isothermal Vertical Cone", Journal of Advanced Research in Fluid Mechanics and Thermal Sciences, Vol. 75(1), pp.1-11, (2021).

[33] Sambath, P., Pullepu, B., Hussain, T., and Shehzad, S.A., "Radiated Chemical Reaction Impacts on Natural Convective MHD Mass Transfer Flow Induced by a Vertical Cone", Results in Physics, Vol. 8, pp. 304-315, (2018).

[34] Mishra, P., Nirmalkar, N., and Chhabra, R., "Free Convection from a Heated Vertical Cone in Generalized Newtonian Fluids", Journal of Thermophysics and Heat Transfer, Vol. 33(1), pp. 1-14, (2019).

[35] Madhavi, K., Prasad, V.R., Subba Rao, A., Anwar Bég, O., and Kadir, A., "Numerical Study of Viscoelastic Micropolar Heat Transfer from a Vertical Cone for Thermal Polymer Coating", Nonlinear Engineering, De Gruyter, Vol. 8(1), (2018).

[36] Huang, C.J., "Effects of Internal Heat Generation and Soret/Dufour on Natural Convection of Non-newtonian Fluids over a Vertical Permeable Cone in a Porous Medium", Journal of King Saud University - Science, Vol. 30(1), pp. 106-111, (2018).

[37] Ajaykumar, M., and Srinivasa, A.H., "Effect of Pressure Work on Free Convection Flow from an Isothermal Truncated Cone with Temperature Dependent Viscosity", Journal of Mathematical and Computational Science, Vol. 10, No. 6, pp. 2422-2433, (2020).

[38] Akbar, N.S., and Butt, A.W., "Ferro-magnetic Effects for Peristaltic Flow of Cu-water Nanofluid for Different Shapes of Nano-size Particles", Applied Nanoscience, Vol. 6, pp. 379-385, (2016).

[39] Sheikholesmi, M., and Bhatti, M.M., "Free Convection of Nanofluid in the Presence of Constant Magnetic Field Considering Shape Effects of Nanoparticles", International Journal of Heat and Mass Transfer, Vol. 111, pp. 1039-1049, (2017).

[40] Haq, R.U., Nadeem, S., Khan, Z.H., and Noor, N.F.M., "Convective Heat Transfer in MHD Slip Flow over a Stretching Surface in the Presence of Carbon Nanotubes", Physica B: Condensed Matter, Vol. 457, pp. 40–47, (2015).

[41] Talley, L.D., Pickard, G.L., Emery, W.J., and Swift, J.H., "*Descriptive Physical Oceanography, Physical Properties of Sea Water*", Sixth Edition, Elsevier Ltd, San Diego, U.S.A., pp. 29–65, (2011).

[42] Pastoriza-Gallego, M., Lugo, L., Legido, J., and Piñeiro, M., "Thermal Conductivity and Viscosity Measurements of Ethylene Glycol-based Al 2O3 Nanofluids", Nanoscale Research Letters, Vol. 6(221), pp. 1–11, (2011).

[43] Aberoumand, S., and Jafarimoghaddam, A., "Experimental Study on Synthesis, Stability, Thermal Conductivity and Viscosity of Cu–engine Oil Nanofluid", Journal of the Taiwan Institute of Chemical Engineers, Vol. 71, pp. 315–322, (2017).

[44] Han, H., Jin, J., and Wu, X., "A Finite-difference Method for the One-dimensional Time-dependent Schrodinger Equation on Unbounded Domain", Computers and Mathematics with Applications, Vol. 50, pp. 1345-1362, (2005).

[45] Thandapani, E., Ragavan, A.R., and Palani, G., "Finite Difference Solution of Unsteady Natural Convection Flow Past a Non-isothermal Vertical Cone under the Influence of Magnetic Field and Thermal Radiation", Journal of Applied Mechanics and Technical Physics, Vol. 53, pp. 408–421, (2012).

[46] Balla, C.S., and Naikoti, K., "Finite Element Analysis of Magnetohydrodynamic Transient Free Convection Flow of Nanofluid over a Vertical Cone with Thermal Radiation", Proceedings of the Institution of Mechanical Engineers, Part N: Journal of Nanoengineering and Nanosystems, pp. 1–13, Institution of Mechanical Engineers (IMechE), (2014).

Nomenclature

B_o electromagnetic induction
c_p specific heat capacity
C species concentration
D species diffusion coefficient
g acceleration due to gravity
Gr Grashof number
Ha Hartmann number/magnetic field parameter
k thermal conductivity
K the absorption coefficient
m shape factor
N buoyancy ratio parameter
p pressure
Pr Prandtl number
Pr Prandtl number
$\bar{p}$ pressure
R Radiation number
Sc Schmidt number
t time
$\bar{T}$ temperature of the fluid
$\bar{u}$ velocity component in x-direction
$\bar{v}$ velocity component in y-direction
U_w fluid inflow velocity at the wall
$\bar{x}$ coordinate axis parallel to the plate
$\bar{y}$ coordinate axis perpendicular to the plate

Symbols

β volumetric extension coefficients
ρ_{nf} density of the nanofluid
ρ_f density of the base fluid
μ_{nf} dynamic viscosity of the nanofluid
ρ_s density of the solid/nanoparticles

ϕ fraction of nanoparticles in the nanofluid
γ Casson parameter
τ shear stress
τ_o Casson yield stress
μ dynamic viscosity
$\dot{\sigma}$ shear rate

Subscript

f fluid
s solid
nf nanofluid
w wall